European Journal of Control 69 (2023) 100763

Contents lists available at ScienceDirect

European Journal of Control

journal homepage: www.elsevier.com/locate/ejcon

Robust adaptive control for formation-based cooperative transportation of a payload by multi quadrotors

Moein Doakhan, Mansour Kabganian*, Ali Azimi

Amirkabir University of Technology, Tehran, Iran

ARTICLE INFO

Article history:
Received 21 September 2021
Revised 4 September 2022
Accepted 20 November 2022
Available online 2 December 2022

Recommended by Prof. T Parisini

Keywords:
Multi-UAV systems
Formation control
Quadrotor
Robust adaptive control
Cooperative transportation

ABSTRACT

This paper discusses the development of position control for a rigid body payload carried by a team of quadrotors in the presence of external disturbance and uncertainty in model parameters. The formation of quadrotors is controlled and maintained during payload transportation for uniform load distribution and collision avoidance. In the controller structure, an adaptive sliding mode hierarchical control with the constant plus proportional rate reaching law is designed to compensate for the uncertainties that have unknown bounds. The finite-time stability of the closed-loop system is performed using Lyapunov stability analysis and the multiple time scale principle. Finally, the simulation results are shown to confirm the performance of the proposed controller in payload trajectory tracking without knowing its mass while the formation of the quadrotors is maintained.

1. Introduction

Autonomous payload transportation is becoming an essential element in human societies, in which robots play a crucial role. Due to the various limitations of ground vehicles, especially in the rapid delivery of the payload to impassable areas, aerial transportation by rotorcraft is recognized as the only possible solution in many cases. Transportation of food and drug, precision spraying in agriculture, extinguishing forest fires, transferring materials between ships, and rescuing people in remote areas are the most critical applications of this problem.

Aerial transportation can be classified into different categories such as aerial grasping [24,33], aerial manipulation [34,36], and cable-suspended [1,2,5–8,10–16,18,20–23,26,28,30,35,37], the latter being a more popular option due to its ease of connection and operation. However, double under-actuated property, highly nonlinear model, and system dynamic coupling cause the controller design to be a complex task, especially when using multi-UAVs, for various reasons, including higher efficiency and reliability. Also, in addition to the disturbance acting on the system, the exact amount of the payload mass properties are sometimes unknown, or payload mass changes during the mission. In such a case, using a robust adaptive controller can be essential.

Cooperative transportation of cable-suspended payload by multiple quadrotors, resulting in fault tolerance, better stability conditions, and higher efficiency in the system, is being investigated using simulations and experimental trials. However, its challenges cause some practical aspects to be omitted or simplified in many cases. Therefore, research on this topic is still ongoing in various aspects such as payload model, desired maneuver, control purpose, and system uncertainties.

Although the cooperative control for a rigid body payload transportation is addressed in [2,10,11,13,16,18,21,23], the payload has been modeled as a point mass to simplify the system in some cases [1,5,8,12,15,20,26,30,35]. In terms of maneuverability, the desired maneuver of the payload is usually slow or in the form of a set point regulation problem, except in a few cases where the problem of trajectory tracking under relatively fast maneuvers has been addressed [8,11,18,21,35].

Cooperative transportation of payload can be considered a multi-objective control problem. If the objective is only transportation, the problem is solved regardless of the importance of UAVs position control relative to each other. However, other objectives can also be considered, such as formation control of UAVs while carrying a payload [2,5,8,10–12,15,16,26,30,35,23]. Although this leads to a more complex control design, it can provide advantages such as uniform load distribution, collision avoidance, preventing the cables' entanglement, and reducing payload swing.

Cooperative payload transportation with formation control of UAVs can be classified into UAV-based (decentralized) and payload-based (centralized). Unlike the decentralized approach, the main

* Corresponding author.
E-mail address: kabgan@aut.ac.ir (M. Kabganian).

https://doi.org/10.1016/j.ejcon.2022.100763
0947-3580/

priority of the system control is payload trajectory tracking, and the system is dynamically coupled in the centralized approach [8,10–12,23,30], which leads to more accurate control of the payload.

In [30], a decentralized controller based on sub-optimal LQR-PID is suggested to maintain the formation of quadrotors for transportation of a point mass payload safely with the minimal swing. In [12], a kinematic formation controller is used to transport a point mass payload with two UAVs considering collision avoidance and uniform load distribution under wind disturbances. A PD controller is designed for the swing control and keeping quadrotors' formation while damping payload oscillations in transporting a point mass payload in [8]; the method introduced requires relative acceleration of payload and quadrotors.

In [23], a centralized dual-space control approach based on the Feedback Linearization (FL) method with a tension distribution algorithm is proposed for cooperative transportation of a rigid body payload with eight quadrotors. In [10,11], a PID hierarchical and centralized controller is introduced in a structure where the payload is defined as the leader for rigid body payload transportation.

In the literature, a common assumption is that the mass properties of the payload are determined and do not change during the mission [1,2,5,8,10–13,16,18,20,21,23,26,30]. However, during the flight, picking up and delivering a payload with an unknown or variable mass may be necessary. So far, a robust adaptive control design is not considered for the cooperative transportation of a cable-suspended rigid body payload under the external disturbance with the centralized formation control. However, this problem has been recently addressed with the decentralized formation approach for a point mass payload [22,37]; it has also been investigated for the cooperative aerial manipulation system [19] and the system of a single quadrotor carrying a payload [6,7,22,29,37].

The main contribution of the present work is the development of a robust adaptive controller to control the rigid body payload position under rapid maneuvers while compensating for the disturbances and uncertainties of the mass properties of a cable-suspended rigid body payload. The control structure of the payload transportation is based on the formation control of quadrotors, which can create potential benefits. The proposed method is based on a sliding mode controller, which does not require knowing the uncertainties. The finite-time stability of the system is proven via the Lyapunov theory. Also, the gain resetting technique has been proposed to compensate for abrupt changes in the payload mass.

The rest of the paper is organized as follows. The dynamic modeling of the system of the cable-suspended rigid body payload with the multiple quadrotors is presented in Section 2. In Section 3, the robust adaptive controller design for trajectory tracking of payload and formation control of quadrotors are presented; and the closed-loop stability analysis of the system is provided via the Lyapunov theory. Section 4 shows the simulation results, and the concluding remarks are presented in Section 5.

2. Problem formulation

2.1. Dynamic modeling

Consider a rigid body payload with mass $m^{\mathcal{P}} \in \mathbb{R}$ and moment of inertia $\mathbf{J}^{\mathcal{P}} \in \mathbb{R}^{3\times3}$ connected by cables to N quadrotors with mass properties $m^{\mathcal{Q}_i} \in \mathbb{R}$ and $\mathbf{J}^{\mathcal{Q}_i} \in \mathbb{R}^{3\times3}$ (Fig. 1).

Remark 1. In mathematical notations, the variables related to the payload, the i th quadrotor, and the i th cable are denoted by superscripts $\mathcal{P}$, $\mathcal{Q}_i$, and $\mathcal{C}_i$, respectively.

Assumption 1. The cables are assumed to be connected to the quadrotors' Center of Mass (CoM) [8,16,18,35]. This assumption is intended only to simplify the dynamic model without losing the generality of the problem. However, it is possible to adjust the CoM of the quadrotors near the cable connection point in practice.

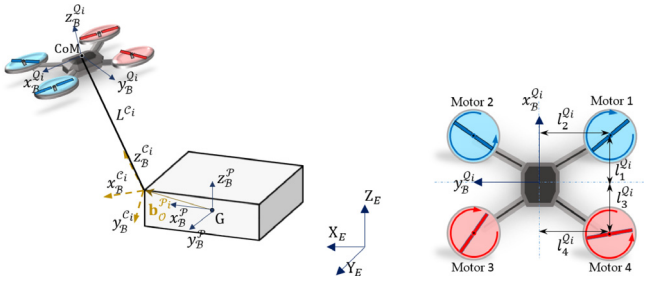

Fig. 1. Problem schematic and reference frames used in the dynamic model.

In this paper, we define the inertial reference frame $X_E Y_E Z_E$, the payload body-fixed frame $x_B^{\mathcal{P}} y_B^{\mathcal{P}} z_B^{\mathcal{P}}$, the i th quadrotor body-fixed frame $x_B^{\mathcal{Q}_i} y_B^{\mathcal{Q}_i} z_B^{\mathcal{Q}_i}$ and the i th cable body-fixed frame $x_B^{\mathcal{C}_i} y_B^{\mathcal{C}_i} z_B^{\mathcal{C}_i}$. The z-axis of the inertial reference frame is considered in the opposite direction of gravity. Also, the CoM of each vehicle (payload and quadrotor) is the frame's origin in all body-fixed frames.

Let $\mathbf{n}^{\mathcal{C}_i} \in \mathbb{R}^3$ be the unit vector corresponding to the direction of the i th cable in the inertial frame and is given by:

$$\mathbf{n}^{\mathcal{C}_i} = \frac{\mathbf{r}_{\mathcal{O}}^{\mathcal{Q}_i} - \mathbf{r}_{\mathcal{O}}^{\mathcal{P}_i}}{L_e^{\mathcal{C}_i}} \tag{1}$$

in which $\mathbf{r}_{\mathcal{O}}^{\mathcal{P}_i} \in \mathbb{R}^3$ and $\mathbf{r}_{\mathcal{O}}^{\mathcal{Q}_i} \in \mathbb{R}^3$ indicate the position of the i th cable connection on the payload and the corresponding quadrotor in the inertial frame, respectively. Also, $L_e^{\mathcal{C}_i} \in \mathbb{R}$ is defined by:

$$L_e^{\mathcal{C}_i} = \left\| \mathbf{r}_{\mathcal{O}}^{\mathcal{Q}_i} - \mathbf{r}_{\mathcal{O}}^{\mathcal{P}_i} \right\|_2 \tag{2}$$

Thus, $\mathbf{r}_{\mathcal{O}}^{\mathcal{P}_i}$ can be calculated as follows:

$$\mathbf{r}_{\mathcal{O}}^{\mathcal{P}_i} = \mathbf{r}_{\mathrm{G}}^{\mathcal{P}} + {}_E^B\mathbf{R}^{\mathcal{P}}\ \mathbf{b}_{\mathcal{O}}^{\mathcal{P}_i} \tag{3}$$

where $\mathbf{r}_{\mathrm{G}} \in \mathbb{R}^3$ is the position of the CoM of the vehicle in the inertial frame, $\mathbf{b}_{\mathcal{O}}^{\mathcal{P}_i} \in \mathbb{R}^3$ is the position of the i th cable connection point in the body-fixed frame of the payload, and ${}_E^B\mathbf{R} \in \mathbb{R}^{3\times3}$ is the rotation matrix of the vehicle from its body-fixed frame to the inertial frame. Moreover, as mentioned before (Assumption 1), it is assumed that:

$$\mathbf{r}_{\mathcal{O}}^{\mathcal{Q}_i} = \mathbf{r}_{\mathrm{G}}^{\mathcal{Q}_i} \tag{4}$$

The dynamic model of the system using the Newton-Euler method is as follows:

$$m^{\mathcal{Q}_i}\ddot{\mathbf{r}}_{\mathrm{G}}^{\mathcal{Q}_i} = m^{\mathcal{Q}_i}\mathbf{g} - T^{\mathcal{C}_i}\mathbf{n}^{\mathcal{C}_i} + {}_E^B\mathbf{R}^{\mathcal{Q}_i}\ \mathbf{f}_{\mathrm{R}}^{\mathcal{Q}_i} + \mathbf{d}_{\mathrm{r}}^{\mathcal{Q}_i} \tag{5}$$

$$\mathbf{J}^{\mathcal{Q}_i}\ \dot{\boldsymbol{\omega}}^{\mathcal{Q}_i} + \boldsymbol{\omega}^{\mathcal{Q}_i} \times \left(\mathbf{J}^{\mathcal{Q}_i}\ \boldsymbol{\omega}^{\mathcal{Q}_i}\right) = \boldsymbol{\tau}_{\mathrm{R}}^{\mathcal{Q}_i} + \mathbf{d}_{\Phi}^{\mathcal{Q}_i} \tag{6}$$

$$m^{\mathcal{P}}\ddot{\mathbf{r}}_{\mathrm{G}}^{\mathcal{P}} = m^{\mathcal{P}}\mathbf{g} + \sum_{i=1}^{N}\left(T^{\mathcal{C}_i}\mathbf{n}^{\mathcal{C}_i}\right) + \mathbf{d}_{\mathrm{r}}^{\mathcal{P}} \tag{7}$$

$$\mathbf{J}^{\mathcal{Q}_i}\ \dot{\boldsymbol{\omega}}^{\mathcal{P}} + \boldsymbol{\omega}^{\mathcal{P}} \times \left(\mathbf{J}^{\mathcal{Q}_i}\ \boldsymbol{\omega}^{\mathcal{P}}\right) = \sum_{i=1}^{N}(\mathbf{b}_{\mathcal{O}}^{\mathcal{P}_i} \times \left(T^{\mathcal{C}_i}\left({}_E^B\mathbf{R}^{\mathcal{P}}\right)^{\mathrm{T}}\mathbf{n}^{\mathcal{C}_i}\right) + \mathbf{d}_{\Phi}^{\mathcal{P}} \tag{8}$$

where:

- $\mathbf{f}_{\mathrm{R}}^{\mathcal{Q}_i} \in \mathbb{R}^3$ and $\boldsymbol{\tau}_{\mathrm{R}}^{\mathcal{Q}_i} \in \mathbb{R}^3$ are the resultant of the rotor forces and moments of the i th quadrotor in its body-fixed frame.
- $\mathbf{d}_{\mathrm{r}}^{\mathcal{Q}_i} \in \mathbb{R}^3$ and $\mathbf{d}_{\Phi}^{\mathcal{Q}_i} \in \mathbb{R}^3$ are aerodynamic forces and moments (wind gust) acting on the CoM of the i th quadrotor, respectively. Also, $\mathbf{d}_{\mathrm{r}}^{\mathcal{P}} \in \mathbb{R}^3$ and $\mathbf{d}_{\Phi}^{\mathcal{P}} \in \mathbb{R}^3$ are aerodynamic forces and moments acting on the CoM of the payload.

- $\boldsymbol{\omega} \in \mathbb{R}^3$ is the angular velocity vector of each vehicle in the body-fixed frame.
- $\mathbf{g} \in \mathbb{R}^3$ is the gravity acceleration in the inertial frame.
- $T^{\mathcal{C}_i} \in \mathbb{R}$ is the norm of tension force of the i th cable.

The thrust force and torque generated by the j-th rotor of a quadrotor, as the primary actuators of the system, can be modeled as follows [25]:

$$F_j = c_T \boldsymbol{\omega}_j^2 \tag{9}$$

$$M_j = c_D \boldsymbol{\omega}_j^2 \tag{10}$$

in which $\boldsymbol{\omega}_j \in \mathbb{R}$ is the angular speed of the j-th rotor. $c_T \in \mathbb{R}$ and $c_D \in \mathbb{R}$ are the thrust force and the drag moment coefficients of each rotor, which are assumed to be identical for all rotors. Also, $l_j^{\mathcal{Q}_i} \in \mathbb{R}; j = 1, \ldots, 4$ indicate the horizontal or vertical distance of the center of rotors to the CoM of the quadrotors, while it is assumed that they are in configuration X, as shown in Fig. 1. Therefore, $\mathbf{f}_{\mathrm{R}}^{\mathcal{Q}_i}$ and $\boldsymbol{\tau}_{\mathrm{R}}^{\mathcal{Q}_i}$ can be defined by the following relations:

$$\mathbf{f}_{\mathrm{R}}^{\mathcal{Q}_i} = \begin{bmatrix} 0 \\ 0 \\ \sum_{j=1}^{4} F_j^{\mathcal{Q}_i} \end{bmatrix} \tag{11}$$

$$\boldsymbol{\tau}_{\mathrm{R}}^{\mathcal{Q}_i} = \begin{bmatrix} l_4^{\mathcal{Q}_i} c_T \left(\left(\boldsymbol{\omega}_3^{\mathcal{Q}_i}\right)^2 - \left(\boldsymbol{\omega}_4^{\mathcal{Q}_i}\right)^2 \right) - l_2^{\mathcal{Q}_i} c_T \left(\left(\boldsymbol{\omega}_1^{\mathcal{Q}_i}\right)^2 - \left(\boldsymbol{\omega}_2^{\mathcal{Q}_i}\right)^2 \right) \\ l_3^{\mathcal{Q}_i} c_T \left(\left(\boldsymbol{\omega}_3^{\mathcal{Q}_i}\right)^2 + \left(\boldsymbol{\omega}_4^{\mathcal{Q}_i}\right)^2 \right) - l_1^{\mathcal{Q}_i} c_T \left(\left(\boldsymbol{\omega}_1^{\mathcal{Q}_i}\right)^2 + \left(\boldsymbol{\omega}_2^{\mathcal{Q}_i}\right)^2 \right) \\ c_D \left(\left(\boldsymbol{\omega}_1^{\mathcal{Q}_i}\right)^2 - \left(\boldsymbol{\omega}_2^{\mathcal{Q}_i}\right)^2 + \left(\boldsymbol{\omega}_3^{\mathcal{Q}_i}\right)^2 - \left(\boldsymbol{\omega}_4^{\mathcal{Q}_i}\right)^2 \right) \end{bmatrix} \tag{12}$$

Assumption 2. It is assumed that the cables are always under tension, and their mass is neglected compared to the other parts' mass [8,18,21,26]. It is logical to assume that the cables are stretched according to the control purpose of uniform load distribution on quadrotors (refer to Section 3).

The norm of the cable tension force is modeled by a spring-damper [26]:

$$T^{\mathcal{C}_i} = k^{\mathcal{C}_i} \left(L_e^{\mathcal{C}_i} - L_0^{\mathcal{C}_i} \right) + c^{\mathcal{C}_i} \left(\dot{L}_e^{\mathcal{C}_i} \right) \tag{13}$$

in which $L_0^{\mathcal{C}_i} \in \mathbb{R}$ is the nominal length of the i th cable, $k^{\mathcal{C}_i} \in \mathbb{R}$ is the spring stiffness coefficient, and $c^{\mathcal{C}_i} \in \mathbb{R}$ is the damping coefficient.

2.2. Model uncertainties

According to the dynamic model developed in Section 2.1, the items considered as uncertainties in the control design (Section 3), the controller must compensate for all, are as follows:

- The wind gust effects ($\mathbf{d}_{\mathrm{r}}^{\mathcal{Q}_i}, \mathbf{d}_{\Phi}^{\mathcal{Q}_i}, \mathbf{d}_{\mathrm{r}}^{\mathcal{P}}, \mathbf{d}_{\Phi}^{\mathcal{P}}$) are presumed as external disturbances.
- The cables' desired tension deviations from actual values and the quadrotors' formation are considered coupling errors between subsystems.
- The parameters of the cable model in Eq. (13) are indeterminate, while there are no external sensors to measure cables' tension.
- The deviations of the quadrotors' actual Euler angles from desired values are considered coupling errors between subsystems.
- The mass properties of quadrotors and payload are uncertain.

3. Control design

The cable-suspended payload with multiple quadrotors is a double underactuated system. In this section, a hierarchical three-loop controller is designed to transport a rigid body payload while maintaining quadrotors formation using the adaptive sliding mode method. It is unnecessary to know the bound of model uncertainties in the proposed approach.

Although generally, the payload is practically a rigid body, controlling its attitude does not matter in some applications, such as carrying a container full of water to extinguish a fire. In such applications, only the control of payload position is essential, while the payload model should be a rigid body. Hence, only rigid body payload position control is essential here.

In summary, the control objectives are as follows:

- First, the trajectory tracking of the payload ($\mathbf{e}_{\mathrm{r}}^{\mathcal{P}} \to 0$);
- Second, maintaining the quadrotors' formation based on the desired attitude of the cables ($\mathbf{e}_{\Phi}^{\mathcal{C}_i} \to 0$).

where $\mathbf{e}_{\mathrm{r}}^{\mathcal{P}}$ is the position error of CoM payload and $\mathbf{e}_{\Phi}^{\mathcal{C}_i}$ is the attitude angle error of the cables relative to the reference direction.

In the controller outer loop, the required resultant force acting on the payload CoM is calculated for its trajectory tracking control. According to the desired formation and the tension force required in each cable, controlling the quadrotors' position is achieved at any time in the middle loop. It is noteworthy that formation-based transportation prevents collisions between the quadrotors and cable entanglement without using complex geometric and optimization solutions. The desired formation of quadrotors is designed based on the attitude angle of the cables and their position relative to the payload. In the inner loop, the attitude of each quadrotor is controlled to track its desired trajectory. The general structure of the proposed control of the system is shown in Fig. 2.

The finite-time stability of each loop is proven separately, and the system's overall stability is accomplished through the multiple time scale principle [9,31]. The detailed analysis for a three-loop hierarchical system is given in [31].

3.1. Payload position control

$\mathbf{u}_{\mathrm{r}}^{\mathcal{P}} \in \mathbb{R}^3$ denotes the resultant of the tension force of the cables connected to the payload in the inertial frame, which is as follows:

$$\mathbf{u}_{\mathrm{r}}^{\mathcal{P}} = \sum_{i=1}^{N} \left(T^{\mathcal{C}_i} \mathbf{n}^{\mathcal{C}_i} \right) \tag{14}$$

It can also be written in the following matrix form:

$$\mathbf{u}_{\mathrm{r}}^{\mathcal{P}} = \mathbf{D}\, \mathbf{f}_{\mathrm{T}} \tag{15}$$

in which $\mathbf{f}_{\mathrm{T}} = [T^{\mathcal{C}_1}, \ldots, T^{\mathcal{C}_N}]^{\mathrm{T}} \in \mathbb{R}^N$, and $\mathbf{D} \in \mathbb{R}^{3\times N}$ is defined as:

$$\mathbf{D} = \left[\mathbf{n}^{\mathcal{C}_1}, \ \ldots, \mathbf{n}^{\mathcal{C}_N} \right] \tag{16}$$

From Eq. (7), the dynamic of translational motion of the payload in the presence of uncertainty $\boldsymbol{\rho}_{\mathrm{r}}^{\mathcal{P}} \in \mathbb{R}^3$ can be presented as:

$$m^{\mathcal{P}} \ddot{\mathbf{r}}_{\mathrm{G}}^{\mathcal{P}} = \mathbf{u}_{\mathrm{r}}^{\mathcal{P}} + m^{\mathcal{P}} \mathbf{g} + \underbrace{\mathbf{d}_{\mathrm{r}}^{\mathcal{P}} + \boldsymbol{\eta}_{\mathrm{r}}^{\mathcal{P}}}_{\boldsymbol{\rho}_{\mathrm{r}}^{\mathcal{P}}} \tag{17}$$

in which $\boldsymbol{\eta}_{\mathrm{r}}^{\mathcal{P}}$ is the coupling error of this subsystem with the translational motion of the quadrotors. This error is due to the cables' actual tension deviation from their desired value and the quadrotors' formation error.

Assumption 3. The uncertainty $\boldsymbol{\rho}_{\mathrm{r}}^{\mathcal{P}}$ in the dynamic model of this subsystem, as well as in other subsystems, is bounded.

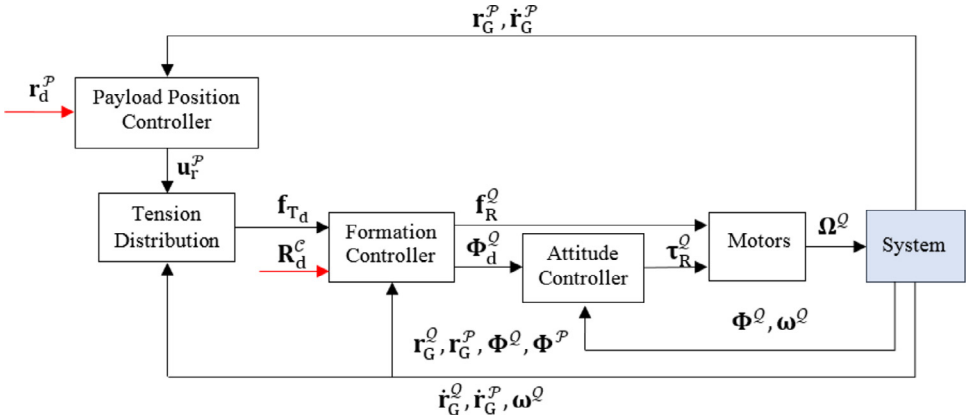

Fig. 2. The controller structure for cooperative payload transportation with the quadrotors' formation control.

Remark 2. Consider two vectors $\mathbf{a} \in \mathbb{R}^n$ and $\mathbf{b} \in \mathbb{R}^n$; $\mathbf{a} \circ \mathbf{b} \in \mathbb{R}^n$ is equal to the Hadamard multiplication of two vectors, whose elements consist of the product of the corresponding elements of $\mathbf{a}$ and $\mathbf{b}$.

Remark 3. For an arbitrary vector such as $\mathbf{s} = [s_1, \ldots, s_n]^{\mathrm{T}} \in \mathbb{R}^n$, we define $\mathrm{sign}(\mathbf{s}) = [\mathrm{sign}(s_1), \ldots, \mathrm{sign}(s_n)]^{\mathrm{T}} \in \mathbb{R}^n$, $|\mathbf{s}| = [|s_1|, \ldots, |s_n|]^{\mathrm{T}} \in \mathbb{R}^n$, and $\mathbf{s}^2 = [s_1^2, \ldots, s_n^2]^{\mathrm{T}} \in \mathbb{R}^n$.

Let $\mathbf{r}_d^{\mathcal{P}} \in \mathbb{R}^3$ be the desired trajectory of the payload, and $\mathbf{e}_r^{\mathcal{P}} = \mathbf{r}_d^{\mathcal{P}} - \mathbf{r}_G^{\mathcal{P}}$ be the vector of the payload position error. The sliding surface of the payload position is defined as follows:

$$\mathbf{s}_r^{\mathcal{P}} = \dot{\mathbf{e}}_r^{\mathcal{P}} + \boldsymbol{\lambda}_r^{\mathcal{P}} \circ \mathbf{e}_r^{\mathcal{P}} \tag{18}$$

in which $\boldsymbol{\lambda}_r^{\mathcal{P}} \in \mathbb{R}^3$ is with positive constants. Thus, the control input $\mathbf{u}_r^{\mathcal{P}}$ with the constant plus proportional rate reaching law considering the uncertainty in the payload mass is as follows:

$$\mathbf{u}_r^{\mathcal{P}} = \hat{m}^{\mathcal{P}} \left(\ddot{\mathbf{r}}_d^{\mathcal{P}} + \boldsymbol{\lambda}_r^{\mathcal{P}} \circ \dot{\mathbf{e}}_r^{\mathcal{P}} + \hat{\mathbf{k}}_r^{\mathcal{P}} \circ \mathbf{s}_r^{\mathcal{P}} + \hat{\mathbf{q}}_r^{\mathcal{P}} \circ \mathrm{sign}\left(\mathbf{s}_r^{\mathcal{P}}\right) - \mathbf{g} \right) \tag{19}$$

where $\hat{m}^{\mathcal{P}} \in \mathbb{R}$ is a nominal value of the payload mass. Therefore, parameter error in the payload mass is denoted by $\tilde{m}^{\mathcal{P}} = \hat{m}^{\mathcal{P}} - m^{\mathcal{P}}$. Also, adaptation laws for the gains $\hat{\mathbf{k}}_r^{\mathcal{P}} \in \mathbb{R}^3$ and $\hat{\mathbf{q}}_r^{\mathcal{P}} \in \mathbb{R}^3$ are designed as:

$$\dot{\hat{\mathbf{q}}}_r^{p} = \boldsymbol{\Gamma}_{q_r}^{\mathcal{P}} \left(\left|\mathbf{s}_r^{\mathcal{P}}\right| \circ \mathrm{sign}\left(\left|\mathbf{s}_r^{\mathcal{P}}\right| - \boldsymbol{\varepsilon}_r^{\mathcal{P}} \right) \right) \tag{20}$$

$$\dot{\hat{\mathbf{k}}}_r^{p} = \boldsymbol{\Gamma}_{k_r}^{\mathcal{P}} \left(\left(\mathbf{s}_r^{\mathcal{P}}\right)^2 \cdot \mathrm{sign}\left(\left|\mathbf{s}_r^{\mathcal{P}}\right| - \boldsymbol{\varepsilon}_r^{\mathcal{P}} \right) \right) \tag{21}$$

where $\boldsymbol{\Gamma}_{q_r}^{\mathcal{P}} \in \mathbb{R}^{3\times3}$, $\boldsymbol{\Gamma}_{k_r}^{\mathcal{P}} \in \mathbb{R}^{3\times3}$ are the arbitrary positive diagonal matrices and $\boldsymbol{\varepsilon}_r^{\mathcal{P}} \in \mathbb{R}^3$ is a constant vector with positive elements. Also, $\hat{\mathbf{q}}_r^{\mathcal{P}}(0)$ and $\hat{\mathbf{k}}_r^{\mathcal{P}}(0)$ should be selected with very small positive constants.

The control law (19) with adaptation laws (20)-(21) guarantees the stability of this subsystem such that the payload tracking errors converge to zero in finite time using Theorems 1 and 2. In Theorems 1, $\mathbf{M} = m^{\mathcal{P}}\mathbf{I}_3$, $\mathbf{b} = m^{\mathcal{P}}\mathbf{I}_3\mathbf{g}$, and $\mathbf{f} = \mathbf{g} = \mathbf{0}$ for this subsystem, with $\mathbf{I}_3$ being an identity matrix of order 3.

Lemma 1. *Suppose $e \in \mathbb{R}$ is the error of state $x \in \mathbb{R}$ in a continuous dynamical system to its equilibrium point, and its sliding surface is given by $s = \dot{e} + \lambda e$, in which $\lambda > 0$. There is a positive constant ξ such that:*

$$|\dot{e}| \le \xi |s| \tag{22}$$

Proof. First, assume $e\dot{e} > 0$, in which case we have:

$$|\dot{e}| \le |\dot{e} + \lambda e| = |s| \tag{23}$$

In this case, the relation $|\dot{e}| \le \xi |s|$ is satisfied for $\xi \ge 1$.

Secondly, suppose $e\dot{e} < 0$, and consider the following Lyapunov function:

$$V = 0.5e^2 \tag{24}$$

Taking the derivative of V results in:

$$\dot{V} = e\dot{e} < 0 \tag{25}$$

Therefore, the system stability is guaranteed, and e is converged to zero. In this case, it is evident that e is always bounded, and condition $|\dot{e}| \le \xi |s|$ satisfies.

Theorem 1. *Consider the following second-order non-linear dynamical system with state vector $\mathbf{x} \in \mathbb{R}^n$ and control input $\mathbf{u} \in \mathbb{R}^n$ under the bounded model uncertainty $\boldsymbol{\rho} \in \mathbb{R}^n$:*

$$\mathbf{M}\,\ddot{\mathbf{x}} = \mathbf{u} + \mathbf{b} + \mathbf{c} \circ \mathbf{f}\left(\mathbf{x}, \dot{\mathbf{x}}\right) + \mathcal{g}\left(\mathbf{x}, \dot{\mathbf{x}}, t\right) + \boldsymbol{\rho} \tag{26}$$

where $\mathbf{M} \in \mathbb{R}^{n\times n}$ is the inertial matrix, and $\mathbf{b} \in \mathbb{R}^n$ and $\mathbf{c} \in \mathbb{R}^n$ are vectors that contain system parameters. Also, $\mathbf{f}(\mathbf{x}, \dot{\mathbf{x}}) \in \mathbb{R}^n$ and $\mathbf{g}(\mathbf{x}, \dot{\mathbf{x}}, t) \in \mathbb{R}^n$ are non-linear functions. Let $\mathbf{x}_d \in \mathbb{R}^n$ and $\mathbf{e} \in \mathbb{R}^n$ be desired state and the error tracking of the system, respectively. $\mathbf{s} = \dot{\mathbf{e}} + \boldsymbol{\lambda} \circ \mathbf{e}$ is defined as the sliding surface of the system, in which $\boldsymbol{\lambda} \in \mathbb{R}^n$ has positive elements. The dynamical system of (26) is finite-time stable under the control law of (27) and adaptation laws of (28)-(29):

$$\mathbf{u} = \hat{\mathbf{M}}\left(\ddot{\mathbf{x}}_d + \boldsymbol{\lambda} \circ \dot{\mathbf{e}} + \hat{\mathbf{k}} \circ \mathbf{s} + \hat{\mathbf{q}} \circ \mathrm{sign}(\mathbf{s}) \right) - \hat{\mathbf{b}} - \hat{\mathbf{c}} \circ \mathbf{f}\left(\mathbf{x}, \dot{\mathbf{x}}\right) - \mathcal{g}\left(\mathbf{x}, \dot{\mathbf{x}}, t\right) \tag{27}$$

$$\dot{\hat{\mathbf{q}}} = \boldsymbol{\Gamma}_q(|\mathbf{s}| \circ \mathrm{sign}(|\mathbf{s}| - \boldsymbol{\varepsilon})) \tag{28}$$

$$\dot{\hat{\mathbf{k}}} = \boldsymbol{\Gamma}_k\left(\mathbf{s}^2 \circ \mathrm{sign}(|\mathbf{s}| - \boldsymbol{\varepsilon})\right) \tag{29}$$

where $\hat{\mathbf{q}} \in \mathbb{R}^n$ and $\hat{\mathbf{k}} \in \mathbb{R}^n$, and $\hat{\mathbf{M}}$, $\hat{\mathbf{b}}$, and $\hat{\mathbf{c}}$ are obtained by replacing the nominal parameters of the system in $\mathbf{M}$, $\mathbf{b}$, and $\mathbf{c}$. Also, $\boldsymbol{\Gamma}_q \in \mathbb{R}^{n\times n}$ and $\boldsymbol{\Gamma}_k \in \mathbb{R}^{n\times n}$ are positive diagonal matrices, and $\boldsymbol{\varepsilon} \in \mathbb{R}^n$ is a constant vector with positive elements.

Proof. Let (27) be replaced in (26):

$$\mathbf{M}\ddot{\mathbf{x}} = \hat{\mathbf{M}}\left(\ddot{\mathbf{x}}_d + \boldsymbol{\lambda} \circ \dot{\mathbf{e}} + \hat{\mathbf{k}} \circ \mathbf{s} + \hat{\mathbf{q}} \circ \mathrm{sign}(\mathbf{s}) \right) - \hat{\mathbf{b}} - \hat{\mathbf{c}} \circ \mathbf{f} + \mathbf{b} + \mathbf{c} \circ \mathbf{f} + \boldsymbol{\rho} \tag{30}$$

The matrix $\mathbf{M}$ (inertia matrix) is practically positive definite, and invertible. Thus, (30) results:

$$\underbrace{\ddot{\mathbf{x}}_d - \ddot{\mathbf{x}} + \boldsymbol{\lambda} \circ \dot{\mathbf{e}}}_{\dot{\mathbf{s}}} + \hat{\mathbf{k}} \circ \mathbf{s} + \hat{\mathbf{q}} \circ \text{sign}(\mathbf{s})$$
$$- \underbrace{(\mathbf{M})^{-1}\Big(\tilde{\mathbf{M}}\Big(\ddot{\mathbf{x}}_d + \boldsymbol{\lambda} \circ \dot{\mathbf{e}} + \hat{\mathbf{k}} \circ \mathbf{s} + \hat{\mathbf{q}} \circ \text{sign}(\mathbf{s})\Big) + \tilde{\mathbf{b}} + \tilde{\mathbf{c}} \circ \mathbf{f} + \boldsymbol{\rho})\Big)}_{\delta}$$
$$= \dot{\mathbf{s}} + \hat{\mathbf{k}} \circ \mathbf{s} + \hat{\mathbf{q}} \circ \text{sign}(\mathbf{s}) - \boldsymbol{\delta} = 0 \tag{31}$$

in which $\tilde{\mathbf{M}} = \mathbf{M} - \hat{\mathbf{M}}$, $\tilde{\mathbf{b}} = \mathbf{b} - \hat{\mathbf{b}}$, and $\tilde{\mathbf{c}} = \mathbf{c} - \hat{\mathbf{c}}$. Assume that $\varrho_i \in \boldsymbol{\varrho}$ is the upper bound of the uncertainty of $\rho_i \in \boldsymbol{\rho}$ such that:

$$\text{diag}(|\boldsymbol{\rho}| - \boldsymbol{\varrho}) \le 0 \tag{32}$$

Using Lemma 1 and based on the definition of $\boldsymbol{\delta} \in \mathbb{R}^n$, we have:

$$|\mathbf{s}^T\boldsymbol{\delta}| \le \underbrace{\left(\left|\mathbf{s}^T\,\tilde{\mathbf{M}}\,\ddot{\mathbf{x}}_d\right| + \left|\mathbf{s}^T\,\tilde{\mathbf{M}}\,\left(\hat{\mathbf{q}} \circ \text{sign}(\mathbf{s})\right)\right| + \left|\mathbf{s}^T(\mathbf{M})^{-1}(\tilde{\mathbf{c}} \circ \mathbf{f})\right| + \left|\mathbf{s}^T(\mathbf{M})^{-1}\tilde{\mathbf{b}}\right| + \left|\mathbf{s}^T(\mathbf{M})^{-1}\boldsymbol{\varrho}\right|\right)}_{\le \boldsymbol{\zeta}^T|\mathbf{s}|} + \underbrace{\left(\left|\mathbf{s}^T\,\tilde{\mathbf{M}}\,\left(\boldsymbol{\lambda} \circ \dot{\mathbf{e}}\right)\right| + \left|\mathbf{s}^T\,\tilde{\mathbf{M}}\,\left(\hat{\mathbf{k}} \circ \mathbf{s}\right)\right|\right)}_{\le \boldsymbol{\xi}^T\mathbf{s}^2} \le \boldsymbol{\zeta}^T|\mathbf{s}| + \boldsymbol{\xi}^T\mathbf{s}^2 \tag{33}$$

in which $\boldsymbol{\zeta} \in \mathbb{R}^n$ and $\boldsymbol{\xi} \in \mathbb{R}^n$ the constant vectors with positive elements, and $\tilde{\mathbf{M}} = \mathbf{M}^{-1}\,\tilde{\mathbf{M}}$. Now consider the following Lyapunov candidate function:

$$V = \frac{1}{2}\mathbf{s}^T\mathbf{s} + \frac{1}{2}\left(\hat{\mathbf{k}} - \mathbf{k}^*\right)^T\mathbf{K}^{-1}\left(\hat{\mathbf{k}} - \mathbf{k}^*\right) + \frac{1}{2}\left(\hat{\mathbf{q}} - \mathbf{q}^*\right)^T\mathbf{Q}^{-1}\left(\hat{\mathbf{q}} - \mathbf{q}^*\right) \tag{34}$$

in which $\mathbf{q}^* \in \mathbb{R}^n$ and $\mathbf{k}^* \in \mathbb{R}^n$ the constant vectors with positive elements and $\mathbf{Q} \in \mathbb{R}^{n\times n}$ and $\mathbf{K} \in \mathbb{R}^{n\times n}$ are positive diagonal matrices. The time derivative of V is as follows:

$$\dot{V} = \mathbf{s}^T\dot{\mathbf{s}} + \tilde{\mathbf{k}}^T\,\mathbf{K}^{-1}\,\dot{\hat{\mathbf{k}}} + \tilde{\mathbf{q}}^T\,\mathbf{Q}^{-1}\,\dot{\hat{\mathbf{q}}} \tag{35}$$

where $\tilde{\mathbf{q}} = \hat{\mathbf{q}} - \mathbf{q}^*$, $\tilde{\mathbf{k}} = \hat{\mathbf{k}} - \mathbf{k}^*$. Using the relations (28), (29), (31), and (33), $\dot{V}$ yields:

$$\dot{V} \le -\hat{\mathbf{q}}^T\,|\mathbf{s}| - \hat{\mathbf{k}}^T\,\mathbf{s}^2 + \boldsymbol{\zeta}^T\,|\mathbf{s}| + \boldsymbol{\xi}^T\,\mathbf{s}^2 + \tilde{\mathbf{q}}^T\,\mathbf{Q}^{-1}\,\boldsymbol{\Gamma}_q$$
$$(|\mathbf{s}| \circ \text{sign}(|\mathbf{s}| - \boldsymbol{\varepsilon})) + \tilde{\mathbf{k}}^T\,\mathbf{K}^{-1}\,\boldsymbol{\Gamma}_k\,\left(\mathbf{s}^2 \circ \text{sign}(|\mathbf{s}| - \boldsymbol{\varepsilon})\right)$$
$$\pm(\mathbf{q}^*)^T|\mathbf{s}| \pm (\mathbf{k}^*)^T\,\mathbf{s}^2 \pm (|\tilde{\mathbf{q}}|)^T\,\mathbf{Y}_q\,|\mathbf{s}| \pm \left(\left|\tilde{\mathbf{k}}\right|\right)^T\,\mathbf{Y}_k\,\mathbf{s}^2 \tag{36}$$

in which $\mathbf{Y}_q \in \mathbb{R}^{n\times n}$ and $\mathbf{Y}_k \in \mathbb{R}^{n\times n}$ are positive diagonal matrices. From Lemma 2, there exists $\mathbf{q}^*$ and $\mathbf{k}^*$ such that always $\text{diag}(\tilde{\mathbf{q}}) < 0$ and $\text{diag}(\tilde{\mathbf{k}}) < 0$. Therefore, (36) can be rewritten as:

$$\dot{V} \le -(|\tilde{\mathbf{q}}|)^T\underbrace{\left(-\mathbf{I}_n + \mathbf{Q}^{-1}\,\boldsymbol{\Gamma}_q\mathbf{S} - \mathbf{Y}_q\right)}_{\mathbf{C}_1 \in \mathbb{R}^{n\times n}}|\mathbf{s}|$$
$$-\left(\left|\tilde{\mathbf{k}}\right|\right)^T\underbrace{\left(-\mathbf{I}_n + \mathbf{K}^{-1}\,\boldsymbol{\Gamma}_k\,\mathbf{S} - \mathbf{Y}_k\right)}_{\mathbf{C}_2 \in \mathbb{R}^{n\times n}}\mathbf{s}^2 - \underbrace{(\mathbf{q}^* - \boldsymbol{\zeta})}_{\mathbf{c}_3 \in \mathbb{R}^n}{}^T|\mathbf{s}|$$
$$-\underbrace{\left(\mathbf{k}^* - \boldsymbol{\xi}\right)}_{\mathbf{c}_3 \in \mathbb{R}^n}{}^T\mathbf{s}^2 - (|\tilde{\mathbf{q}}|)^T\,\mathbf{Y}_q\,|\mathbf{s}| - \left(\left|\tilde{\mathbf{k}}\right|\right)^T\,\mathbf{Y}_k\,\mathbf{s}^2 \tag{37}$$

where $\mathbf{S} = \text{diag}(\text{sign}(|\mathbf{s}| - \boldsymbol{\varepsilon})) \in \mathbb{R}^{n\times n}$. In case 1, suppose that the matrix of $\text{diag}(|\mathbf{s}| - \boldsymbol{\varepsilon}) > 0$. $\mathbf{C}_1 \in \mathbb{R}^{n\times n}$ and $\mathbf{C}_2 \in \mathbb{R}^{n\times n}$ are positive definite by selecting $\mathbf{Q}$ and $\mathbf{K}$ so that $\mathbf{A}_Q = \boldsymbol{\Gamma}_q(\mathbf{Y}_q + \mathbf{I}_n)^{-1} - \mathbf{Q}$ and $\mathbf{A}_K = \boldsymbol{\Gamma}_k(\mathbf{Y}_k + \mathbf{I}_n)^{-1} - \mathbf{K}$ are the positive definite matrices. In addition, there exist $\mathbf{q}^*$ and $\mathbf{k}^*$ such that $\text{diag}(\mathbf{c}_3) > 0$ and $\text{diag}(\mathbf{c}_4) > 0$. Therefore, it results in:

$$\dot{V} \le -\sqrt{2}|\mathbf{s}|^T\frac{\mathbf{c}_3}{\sqrt{2}} - \sqrt{2}(|\tilde{\mathbf{q}}|)^T\left(\mathbf{Q}^{-\frac{1}{2}}\,\mathbf{Q}^{\frac{1}{2}}\right)\mathbf{C}_1\frac{\boldsymbol{\varepsilon}}{\sqrt{2}} - \sqrt{2}\left(\left|\tilde{\mathbf{k}}\right|\right)^T$$
$$\left(\mathbf{K}^{-\frac{1}{2}}\,\mathbf{K}^{\frac{1}{2}}\right)\mathbf{C}_2\frac{\boldsymbol{\varepsilon}^2}{\sqrt{2}} \le -\gamma\sqrt{\frac{1}{2}\left(\mathbf{s}^T\,\mathbf{s} + \tilde{\mathbf{q}}^T\,\mathbf{Q}^{-1}\,\tilde{\mathbf{q}} + \tilde{\mathbf{k}}^T\,\mathbf{K}^{-1}\,\tilde{\mathbf{k}}\right)}$$
$$\le -\gamma\,V^{1/2} \tag{38}$$

in which:

$$\gamma = -\min\left(\min\left(\sqrt{2}\,\mathbf{c}_3\right),\ \min\left(\sqrt{2}\ \mathbf{Q}^{1/2}\,\mathbf{C}_1\,\boldsymbol{\varepsilon}\right), \min\left(\sqrt{2}\ \mathbf{K}^{1/2}\,\mathbf{C}_2\boldsymbol{\varepsilon}^2\right)\right) \tag{39}$$

Thus, the finite-time convergence of the system to a domain of $\text{diag}(|\mathbf{s}| - \boldsymbol{\varepsilon}) < 0$ is guaranteed from any initial condition $\text{diag}(|\mathbf{s}(0)| - \boldsymbol{\varepsilon}) > 0$ using the above equations and Theorem 2. In case 2, the sign of V for $\text{diag}(|\mathbf{s}| - \boldsymbol{\varepsilon}) \le 0$ is indistinct. Therefore, $|\mathbf{s}|$ may be increased until $\text{diag}(|\mathbf{s}| - \boldsymbol{\varepsilon}) > 0$, which restores case 1 and conditions of finite-time stability [27]. Selecting the value of $\boldsymbol{\varepsilon}$ is vital because a too-small value causes high oscillation, and a too-large value leads to less controller accuracy [27].

Remark 4. For a positive diagonal matrix $\mathbf{Q} = \text{diag}([q_1, \ldots, q_n]) \in \mathbb{R}^{n\times n}$, $\mathbf{Q}^{1/2} \in \mathbb{R}^{n\times n}$ and $\mathbf{Q}^{-1/2} \in \mathbb{R}^{n\times n}$ are defined as $\text{diag}([\sqrt{q_1}, \ldots, \sqrt{q_n}])$ and inverse of $\mathbf{Q}^{1/2}$, respectively.

Lemma 2. *Consider the dynamical system (26) with the control input (27)-(28); there are positive constants $\mathbf{q}^*$ and $\mathbf{k}^*$ so that there are always $\text{diag}(\hat{\mathbf{q}}(t) - \mathbf{q}^*) \le 0$ and $\text{diag}(\hat{\mathbf{q}}(t) - \mathbf{k}^*) \le 0$.*

Proof. According to the sliding surface dynamic in (31), all the components of $\boldsymbol{\delta}$ are assumed to be bounded. Thus, this Lemma can be proved in [27] for $\text{diag}(\hat{\mathbf{q}}(t) - \mathbf{q}^*) \le 0$; it is straightforward to extend for $\text{diag}(\hat{\mathbf{k}}(t) - \mathbf{k}^*) \le 0$.

Remark 5. To avoid over-reducing the value of adaptation gains $\hat{q}_i \in \hat{\mathbf{q}}$ and $\hat{k}_i \in \hat{\mathbf{k}}$, the adaptation laws can be modified as follows [27]:

$$\dot{\hat{q}}_i(t) = \begin{cases} \Gamma_{q_i}(|s_i|\text{sign}(|s_i| - \varepsilon_i)), & \hat{q}_i(t) \ge \hat{q}_i(0) \\ \hat{q}_i(0), & \hat{q}_i(t) < \hat{q}_i(0) \end{cases} \tag{40}$$

$$\dot{\hat{k}}_i(t) = \begin{cases} \Gamma_{k_i}\left(s_i^2\text{sign}(|s_i| - \varepsilon_i)\right), & \hat{k}_i(t) \ge \hat{k}_i(0) \\ \hat{k}_i(0), & \hat{k}_i(t) < \hat{k}_i(0) \end{cases} \tag{41}$$

Remark 6. The $\text{sign}(s_i)$ function in the sliding mode control law (27) leads to chattering, which can be reduced by using a boundary layer $\mu_i > 0$ in the neighboring of the sliding surface. Thus the $\text{sat}(s_i)$ function can be suggested instead of $\text{sign}(s_i)$ [32]:

$$\text{sat}(s_i) = \begin{cases} sign(s_i), & |s_i| \ge \mu_i \\ \frac{s_i}{\mu_i}, & |s_i| < \mu_i \end{cases} \tag{42}$$

Theorem 2. *[4]. Consider the following continuous dynamical system:*

$$\dot{x} = \text{f}(x) \tag{43}$$

If the Lyapunov function $V(x) > 0$ exists such that always:

$$\dot{V}(x) < -\gamma\,V^p(\S) \tag{44}$$

in which $\gamma > 0$ and $p \in (0, 1)$, then the system is the globally finite-time stable at the equilibrium point, and the settling time t_s satisfies the following relation:

$$t_s \le \frac{V^{1-p}(x(0))}{\gamma(1-p)} \tag{45}$$

3.2. Quadrotors formation control

In practice, the resultant force applied to the payload must be provided by controlling the tension force of the cables. Using $\mathbf{u}_{\mathrm{r}}^{\mathcal{P}}$ in the controller's outer loop and the quadrotors' desired formation, each cable's magnitude of desired tension can be determined with Eq. (15). In this work, the desired formation of the quadrotors is controlled based on their position relative to the payload and cables' angles.

Let $T_{\mathrm{d}}^{\mathcal{C}_i} \in \mathbb{R}$ be the desired tension of the i th cable and $\mathbf{f}_{\mathrm{T_d}} = [T_{\mathrm{d}}^{\mathcal{C}_1}, \ldots, T_{\mathrm{d}}^{\mathcal{C}_N}]^{\mathrm{T}} \in \mathbb{R}^N$, which are calculated as follows based on the inverse of the following Equation:

$$\mathbf{u}_{\mathrm{r}}^{\mathcal{P}} = \mathbf{D}_{\mathrm{d}} \mathbf{f}_{\mathrm{T_d}} \tag{46}$$

where $\mathbf{D}_{\mathrm{d}} \in \mathbb{R}^{3\times N}$ is similar to Eq. (16), with the difference that the quadrotors' desired formation is used instead of the current formation. This relationship is called the tension distribution in the control structure of the system (Fig. 2). The matrix $\mathbf{D}_{\mathrm{d}}$ is non-square for $N \geq 4$. Therefore, the linear system of Eq. (46) has infinitely many solutions if $N \geq 4$ and $\mathrm{rank}(\mathbf{D}_{\mathrm{d}}) = 3$ (Assumption 4). In practice, $T_{\mathrm{d}}^{\mathcal{C}_i}$ is constrained by upper and lower bounds:

$$0 \leq T_{\mathrm{d}}^{\mathcal{C}_i} \leq T_{max} \tag{47}$$

Thus, the feasible solutions set of $\mathbf{f}_{\mathrm{T_d}}$ is limited by this constraint. On the other hand, to distribute the load evenly on the quadrotors, the following cost function minimization is proposed in an optimization problem:

$$\text{minimize } J: \frac{1}{2}\left(\mathbf{f}_{\mathrm{T_d}}\right)^{\mathrm{T}} \mathbf{A} \left(\mathbf{f}_{\mathrm{T_d}}\right) \tag{48}$$

in which $\mathbf{A} \in \mathbb{R}^{N\times N}$ is a positive definite diagonal matrix for weighting each quadrotor. By default, it is taken as an identity matrix.

The form of the quadratic cost function (48), the linear inequality constraint (47), and linear equality constraint (46) in this problem lead to a Quadratic Programming (QP) problem, which can be solved in a variety of methods [3,17].

Assumption 4. It is supposed that by using a proper formation with four quadrotors, direction vectors of the cables will form a matrix $\mathbf{D}_{\mathrm{d}}$ with full row rank (rank 3). This assumption can permanently be established by choosing a suitable and feasible formation.

Theorem 3. *The optimization problem of Eq. (48) with the equality constraint (46) has a unique minimum point under Assumption 4.*

Proof. The feasible set of this problem is a convex set, and the cost function (48) is a strictly convex function, as its Hessian is positive definite [3]. Therefore, the first-order necessary conditions for a local minimum point are also sufficient conditions for the global minimum point [3], which can be written with Lagrange multipliers as:

$$\mathbf{K}\begin{bmatrix}\mathbf{f}_{\mathrm{T_d}} \\ \boldsymbol{\lambda}_{\mathrm{L}}\end{bmatrix} = \begin{bmatrix}\mathbf{0}_{4\times 1} \\ \mathbf{u}_{\mathrm{r}}^{\mathcal{P}}\end{bmatrix} \tag{49}$$

where:

$$\mathbf{K} = \begin{bmatrix}\mathbf{A} & \mathbf{D}_{\mathrm{d}}^{\mathrm{T}} \\ \mathbf{D}_{\mathrm{d}} & \mathbf{0}\end{bmatrix} \tag{50}$$

and $\boldsymbol{\lambda}_{\mathrm{L}} \in \mathbb{R}^{3\times 1}$ is the vector of Lagrange multipliers. The existence and uniqueness condition of the solution is that the determinant of $\mathbf{K}$ is not zero. Consider the relation below:

$$\det(\mathbf{K}) = \det(\mathbf{A}).\det\left(\mathbf{D}_{\mathrm{d}}\ \mathbf{A}^{-1}\ \mathbf{D}_{\mathrm{d}}^{\mathrm{T}}\right) \tag{51}$$

Noting that $\mathbf{A}$ is positive definite and $\mathbf{D}_{\mathrm{d}}$ is full row-rank, the determinant of $\mathbf{K}$ cannot be zero; therefore, the solution exists and is unique.

The tension force of the cables must be supplied by the control of thrust and relative position of quadrotors. Let the reference direction of each cable be defined parallel to the z-axis of the inertial frame; $\mathbf{R}^{\mathcal{C}_i} \in \mathbb{R}^{3\times 3}$ is the rotation matrix to align the direction of the i th cable from Euler angles $\psi^{\mathcal{C}_i}$-$\theta^{\mathcal{C}_i}$-$\phi^{\mathcal{C}_i}$ with Z-Y-X sequence to its reference direction.

Let $\mathbf{R}_{\mathrm{d}}^{\mathcal{C}_i}$ be the rotation matrix $\mathbf{R}^{\mathcal{C}_i}$ as determined by the desired Euler angle of the cables $\phi_{\mathrm{d}}^{\mathcal{C}_i}$, $\theta_{\mathrm{d}}^{\mathcal{C}_i}$, and $\psi_{\mathrm{d}}^{\mathcal{C}_i}$, which $\psi_{d}^{\mathcal{C}_i} = \psi^{\mathcal{P}}$ by the assumption of no twisting of cables. Therefore, the quadrotors' desired position can be determined as a function of the cables' desired direction by the following equation:

$$\mathbf{r}_{\mathrm{d}}^{\mathcal{Q}_i} = \mathbf{r}_{\mathcal{O}}^{\mathcal{P}_i} + \mathbf{R}_{\mathrm{d}}^{\mathcal{C}_i}\ \mathbf{b}_{\mathcal{O}}^{\mathcal{C}_i} \tag{52}$$

where $\mathbf{b}_{\mathcal{O}}^{\mathcal{C}_i} = [0, 0, L_e^{\mathcal{C}_i}]^{\mathrm{T}}$. From Eq. (5), we have:

$$m^{\mathcal{Q}_i}\ddot{\mathbf{r}}_{\mathrm{G}}^{\mathcal{Q}_i} = \mathbf{u}_{\mathrm{r}}^{\mathcal{Q}_i} - T_{\mathrm{d}}^{\mathcal{C}_i}\mathbf{n}^{\mathcal{C}_i} + m^{\mathcal{Q}_i}\mathbf{g} + \underbrace{\mathbf{d}_{\mathrm{r}}^{\mathcal{Q}_i} + \boldsymbol{\eta}_{\mathrm{r}}^{\mathcal{Q}_i}}_{\boldsymbol{\rho}_{\mathrm{r}}^{\mathcal{Q}_i}} \tag{53}$$

where $\boldsymbol{\eta}_{\mathrm{r}}^{\mathcal{Q}_i} \in \mathbb{R}^3$ is included in the coupling error due to the quadrotors' actual attitude deviation from their desired values and the cables' model uncertainty. Thus, $\boldsymbol{\rho}_{\mathrm{r}}^{\mathcal{Q}_i} \in \mathbb{R}^3$ is bounded similarly to Assumption 3. Also, $\mathbf{u}_{\mathrm{r}}^{\mathcal{Q}_i} \in \mathbb{R}^3$ is given by:

$$\mathbf{u}_{\mathrm{r}}^{\mathcal{Q}_i} = {}_{E}^{\mathcal{B}}\mathbf{R}^{\mathcal{Q}_i}\ \mathbf{f}_{\mathrm{R}}^{\mathcal{Q}_i} = \begin{bmatrix}\left(\cos\phi^{\mathcal{Q}_i}\sin\theta^{\mathcal{Q}_i}\cos\psi^{\mathcal{Q}_i} + \sin\phi^{\mathcal{Q}_i}\sin\psi^{\mathcal{Q}_i}\right)\mathcal{T}^{\mathcal{Q}_i} \\ \left(\cos\phi^{\mathcal{Q}_i}\sin\theta^{\mathcal{Q}_i}\sin\psi^{\mathcal{Q}_i} - \sin\phi^{\mathcal{Q}_i}\cos\psi^{\mathcal{Q}_i}\right)\mathcal{T}^{\mathcal{Q}_i} \\ \left(\cos\phi^{\mathcal{Q}_i}\cos\theta^{\mathcal{Q}_i}\right)\mathcal{T}^{\mathcal{Q}_i}\end{bmatrix} \tag{54}$$

where $\mathcal{T}^{\mathcal{Q}_i} = \sum_{j=1}^{4} F_j^{\mathcal{Q}_i}$. The sliding surface of the i th quadrotor $\mathbf{s}_{\mathrm{r}}^{\mathcal{Q}_i} \in \mathbb{R}^3$ is defined similarly to Eq. (18) by its position error $\mathbf{e}_{\mathrm{r}}^{\mathcal{Q}_i} = \mathbf{r}_{\mathrm{d}}^{\mathcal{Q}_i} - \mathbf{r}_{\mathrm{G}}^{\mathcal{Q}_i}$. The control input $\mathbf{u}_{\mathrm{r}}^{\mathcal{Q}_i}$, with a structure similar to (27), is designed as follows:

$$\mathbf{u}_{\mathrm{r}}^{\mathcal{Q}_i} = \hat{m}^{\mathcal{Q}_i}\left(\ddot{\mathbf{r}}_{\mathrm{d}}^{\mathcal{Q}_i} + \boldsymbol{\lambda}_{\mathrm{r}}^{\mathcal{Q}_i} \circ \dot{\mathbf{e}}_{\mathrm{r}}^{\mathcal{Q}_i} + \hat{\mathbf{k}}_{\mathrm{r}}^{\mathcal{Q}_i} \circ \mathbf{s}_{\mathrm{r}}^{\mathcal{Q}_i} + \hat{\mathbf{q}}_{\mathrm{r}}^{\mathcal{Q}_i} \circ \mathrm{sign}\left(\mathbf{s}_{\mathrm{r}}^{\mathcal{Q}_i}\right) - \mathbf{g}\right) + T_{\mathrm{d}}^{\mathcal{C}_i}\mathbf{n}^{\mathcal{C}_i} \tag{55}$$

where $\hat{m}^{\mathcal{Q}_i}$ is the nominal value of the i th quadrotor mass. Also, the adaptation gains $\hat{\mathbf{k}}_{\mathrm{r}}^{\mathcal{Q}_i} \in \mathbb{R}^3$and $\hat{\mathbf{q}}_{\mathrm{r}}^{\mathcal{Q}_i} \in \mathbb{R}^3$are designed according to adaptation laws introduced in (28) and (29). Therefore, using $\mathbf{M} = m^{\mathcal{Q}_i}\mathbf{I}_3$, $\mathbf{b} = m^{\mathcal{Q}_i}\mathbf{I}_3\mathbf{g}$, $\mathbf{f} = \mathbf{0}$, and $\mathcal{g} = -T_{\mathrm{d}}^{\mathcal{C}_i}\mathbf{n}^{\mathcal{C}_i}$ in Theorem 1, the finite-time stability of this subsystem is proved.

As mentioned, quadrotor formations are based on the attitude angle of their cables. In other words, $\mathbf{e}_{\mathrm{r}}^{\mathcal{Q}_i} \to \mathbf{0}$ is equivalent to $\mathbf{e}_{\Phi}^{\mathcal{C}_i} \to \mathbf{0}$, which $\mathbf{e}_{\Phi}^{\mathcal{C}_i} = [\phi_{\mathrm{d}}^{\mathcal{C}_i}, \theta_{\mathrm{d}}^{\mathcal{C}_i}]^{\mathrm{T}} - [\phi^{\mathcal{C}_i}, \theta^{\mathcal{C}_i}]^{\mathrm{T}}$.

3.3. Quadrotors attitude control

Recalling that a quadrotor is an underactuated system, its position control is performed through attitude control. Let $\psi_{\mathrm{d}}^{\mathcal{Q}_i}$ be the desired yaw angle of the i th quadrotor and $\mathbf{u}_{\mathrm{r}}^{\mathcal{Q}_i} = [u_{\mathrm{r}_1}^{\mathcal{Q}_i}, u_{\mathrm{r}_2}^{\mathcal{Q}_i}, u_{\mathrm{r}_3}^{\mathcal{Q}_i}]^{\mathrm{T}}$ is defined based on (55). According to Eq. (54), the desired roll and pitch angles of the quadrotor for its desired position are calculated as follows:

$$\phi_{\mathrm{d}}^{\mathcal{Q}_i} = \mathrm{f}_{\phi}\left(\mathbf{u}_{\mathrm{r}}^{\mathcal{Q}_i}, \psi_{\mathrm{d}}^{\mathcal{Q}_i}\right) = \tan^{-1}\left(\frac{u_{\mathrm{r}_1}^{\mathcal{Q}_i}\sin\psi_{\mathrm{d}}^{\mathcal{Q}_i} - u_{\mathrm{r}_2}^{\mathcal{Q}_i}\cos\psi_{\mathrm{d}}^{\mathcal{Q}_i}}{\sqrt{\left(u_{\mathrm{r}_1}^{\mathcal{Q}_i}\cos\psi_{\mathrm{d}}^{\mathcal{Q}_i} + u_{\mathrm{r}_2}^{\mathcal{Q}_i}\sin\psi_{\mathrm{d}}^{\mathcal{Q}_i}\right)^2 + \left(u_{\mathrm{r}_3}^{\mathcal{Q}_i}\right)^2}}\right) \tag{56}$$

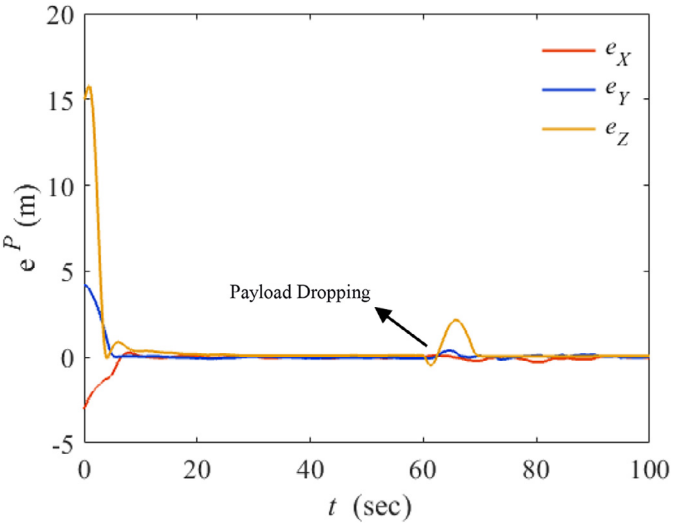

Fig. 3. Payload trajectory tracking error with the ASM.

$$\theta_{\mathrm{d}}^{\mathcal{Q}_i} = \mathrm{f}_\theta\left(\mathbf{u}_{\mathrm{r}}^{\mathcal{Q}_i}, \psi_{\mathrm{d}}^{\mathcal{Q}_i}\right) = \tan^{-1}\left(\frac{u_{\mathrm{r}_1}^{\mathcal{Q}_i}\cos\psi_{\mathrm{d}}^{\mathcal{Q}_i} + u_{\mathrm{r}_2}^{\mathcal{Q}_i}\sin\psi_{\mathrm{d}}^{\mathcal{Q}_i}}{u_{\mathrm{r}_2}^{\mathcal{Q}_i}}\right) \tag{57}$$

Assumption 5. Quadrotors do not perform acrobatic maneuvers of roll and pitch. Therefore, their angular velocity in the body frame is assumed to be equal to the rate of change of Euler angles:

$$\boldsymbol{\omega}^{\mathcal{Q}_i} = \dot{\boldsymbol{\Phi}}^{\mathcal{Q}_i} \tag{58}$$

in which $\boldsymbol{\Phi}^{\mathcal{Q}_i} = [\phi^{\mathcal{Q}_i}, \theta^{\mathcal{Q}_i}, \psi^{\mathcal{Q}_i}\ ]^{\mathrm{T}}$. This assumption is only considered in the control design of quadrotors' attitude as a common assumption for quadrotors. However, the model of this subsystem is under the general form of Eq. (6) in the simulation.

The quadrotor rotational dynamics (8) can be written by Assumption 5 as follows:

$$\mathbf{J}^{\mathcal{Q}_i}\ \ddot{\boldsymbol{\Phi}}^{\mathcal{Q}_i} = \mathbf{u}_{\Phi}^{\mathcal{Q}_i} - \dot{\boldsymbol{\Phi}}^{\mathcal{Q}_i} \times \left(\mathbf{J}^{\mathcal{Q}_i}\ \dot{\boldsymbol{\Phi}}^{\mathcal{Q}_i}\right) + \boldsymbol{\rho}_{\Phi}^{\mathcal{Q}_i} \tag{59}$$

in which $\boldsymbol{\rho}_{\Phi}^{\mathcal{Q}_i} = \mathbf{d}_{\Phi}^{\mathcal{Q}_i}$ and $\mathbf{u}_{\Phi}^{\mathcal{Q}_i} = \boldsymbol{\tau}_{\mathrm{R}}^{\mathcal{Q}_i}$. Let $\mathbf{e}_{\Phi}^{\mathcal{Q}_i} = \boldsymbol{\Phi}_{\mathrm{d}}^{\mathcal{Q}_i} - \boldsymbol{\Phi}^{\mathcal{Q}_i}$ be the attitude error of the i th quadrotor and $\mathbf{s}_{\Phi}^{\mathcal{Q}_i} \in \mathbb{R}^3$ be its sliding surface

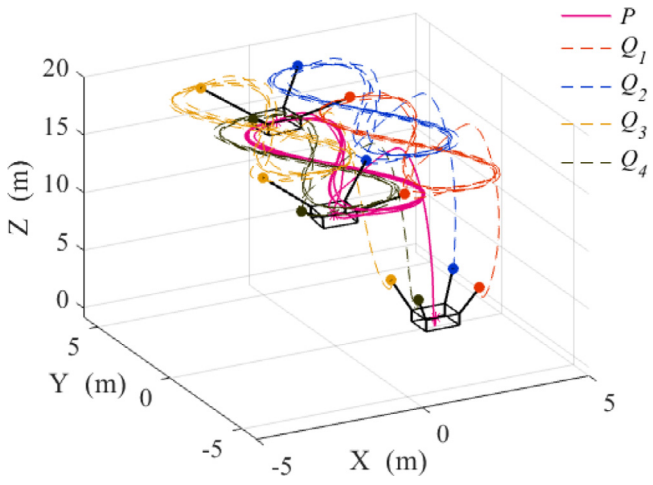

Fig. 5. 3D trajectory of the system with the ASM controller.

similar to Eq. (18); $\mathbf{u}_{\Phi}^{\mathcal{Q}_i}$ is designed using Eq. (27) as follows:

$$\mathbf{u}_{\Phi}^{\mathcal{Q}_i} = \hat{\mathbf{J}}^{\mathcal{Q}_i}\left(\ddot{\boldsymbol{\Phi}}_{\mathrm{d}}^{\mathcal{Q}_i} + \boldsymbol{\lambda}_{\Phi}^{\mathcal{Q}_i} \circ \dot{\mathbf{e}}_{\Phi}^{\mathcal{Q}_i} + \hat{\mathbf{k}}_{\Phi}^{\mathcal{Q}_i} \circ \mathbf{s}_{\Phi}^{\mathcal{Q}_i} + \hat{\mathbf{q}}_{\Phi}^{\mathcal{Q}_i} \circ \mathrm{sign}\left(\mathbf{s}_{\Phi}^{\mathcal{Q}_i}\right)\right) + \dot{\boldsymbol{\Phi}}^{\mathcal{Q}_i} \times \left(\hat{\mathbf{J}}^{\mathcal{Q}_i}\ \dot{\boldsymbol{\Phi}}^{\mathcal{Q}_i}\right) \tag{60}$$

where $\hat{\mathbf{J}}^{\mathcal{Q}_i}$ is the nominal inertia matrix of the i th quadrotor. Also, adaptation gains $\hat{\mathbf{k}}_{\Phi}^{\mathcal{Q}_i} \in \mathbb{R}^3$ and $\hat{\mathbf{q}}_{\Phi}^{\mathcal{Q}_i} \in \mathbb{R}^3$ are designed based on adaptation laws introduced in (28) and (29). For this subsystem, $\mathbf{M} = \mathbf{J}^{\mathcal{Q}_i}$, $\mathbf{b} = \mathbf{0}$, $\mathbf{c} \circ \mathbf{f} = -\dot{\boldsymbol{\Phi}}^{\mathcal{Q}_i} \times (\mathbf{J}^{\mathcal{Q}_i}\ \dot{\boldsymbol{\Phi}}^{\mathcal{Q}_i})$, and $\mathbf{G} = \mathbf{0}$ in Theorem 1.

4. Simulation results

This section illustrates the performance of the proposed approach through a simulation example. The simulation scenario is that the nominal values of all the mass parameters of the system have 50% uncertainty compared to their actual values, and the system is under external disturbances. Also, the payload mass abruptly changes (about 80% reduction) at $t = 60$ sec (the payload dropping time) during the maneuver.

The external disturbance is modeled with a wind gust model of the MATLAB software. The range of disturbance on the translational dynamics of quadrotors and payload is ±2 N and ±10 N, respectively. These values are ±0.005 N.m and ±0.01 N.m in the

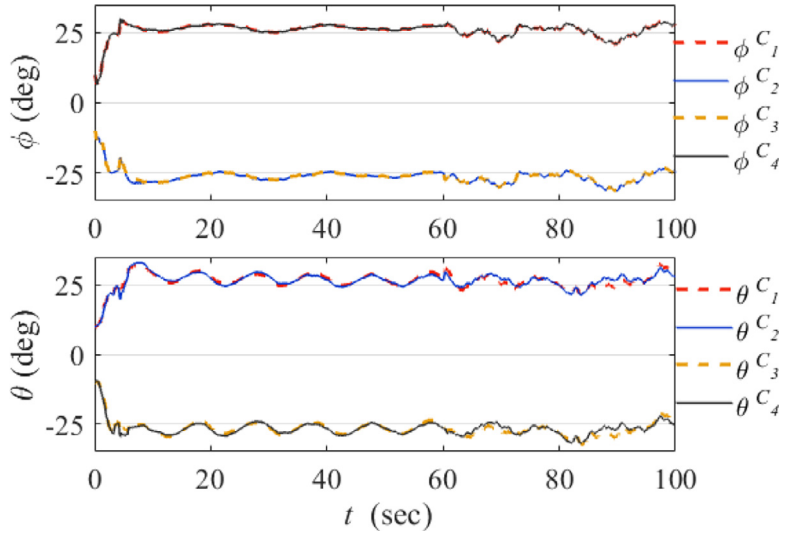

Fig. 4. The cables attitude angles with the ASM controller.

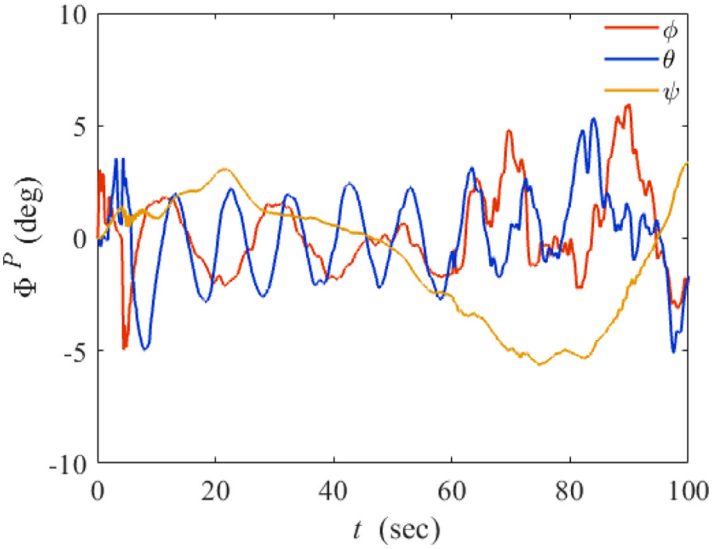

Fig. 6. The payload attitude based on Euler angles with the ASM controller.

Table 1
Compare the performance of controller ASM with SM and FL.

Controller	Case	RMS of payload tracking error (m)			
		X	Y	Z	magnitude
ASM	Before the payload dropping	0.042	0.039	0.154	0.16
SM		0.455	0.635	8.49	8.53
FL		9.37	6.24	15.87	19.46
ASM	After the payload dropping	0.113	0.077	0.059	0.15
SM		0.089	0.172	0.309	0.36
FL		10.98	8.86	0.84	14.13

quadrotors and payload rotational dynamics. These disturbances can create intensive instability effects after reducing the mass of the payload ($t > 60$).

In this example, the following parameters are used for all quadrotors: $m^{\mathcal{Q}_i} = 4$ kg, $\mathbf{J}^{\mathcal{Q}_i} = \text{diag}(0.05,\ 0.05,\ 0.075)$ kg.m^2, $l_1^{\mathcal{Q}_i} = l_2^{\mathcal{Q}_i} = l_3^{\mathcal{Q}_i} = l_4^{\mathcal{Q}_i} = 0.4$ m. The parameters of the rotors are $c_T = 1.05 \times 10^{-4}$N.s^2 and $c_D = 2.1 \times 10^{-6}$N.m.s^2, and their dynamic as a DC motor is modeled with a first-order low pass filter as follows [2]:

$$\frac{20}{s+20} \tag{61}$$

The payload has a cube shape with a side length of 1.0 m with time-varying mass properties. The initial value of payload parameters are $m^{\mathcal{P}} = 12kg$ and $J^{\mathcal{P}} = diag(0.3, 0.3, 0.65)kg \cdot m^2$, which abruptly changes to $m^{\mathcal{P}} = 2.5$ kg and $\mathbf{J}^{\mathcal{P}} = \text{diag}(0.15,\ 0.15,\ 0.32)$ kg.m^2 in the payload dropping time. The cables are modeled with $k^{\mathcal{C}} = 100\frac{\text{kN}}{\text{m}}$, $c^{\mathcal{C}} = 200\ \frac{\text{N.s}}{\text{m}}$, $L_0^{\mathcal{C}} = 2.5$ m and are connected to the upper surface corners of the payload. The payload reference trajectory, similar to [18], is chosen as:

$$\mathbf{r}_{\text{d}}^{\mathcal{P}} = \begin{bmatrix} 1.2sin(0.2\pi t) \\ 4.2cos(0.1\pi t) \\ 15 \end{bmatrix} \text{m}$$

The initial position of the payload is $\mathbf{r}_{\text{G}}^{\mathcal{P}}(0) = [3,\ 0,\ 0]^{\text{T}}$ m and its initial attitude and velocity are equal to zero. It has already been mentioned that the quadrotors formation is created by controlling their position relative to the payload. In other words, the desired formation of quadrotors is controlled through the attitude

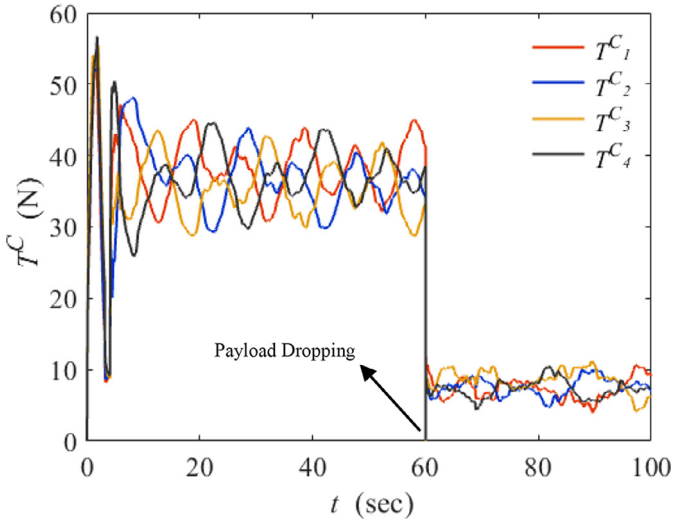

Fig. 7. The tension force of cables with the ASM controller.

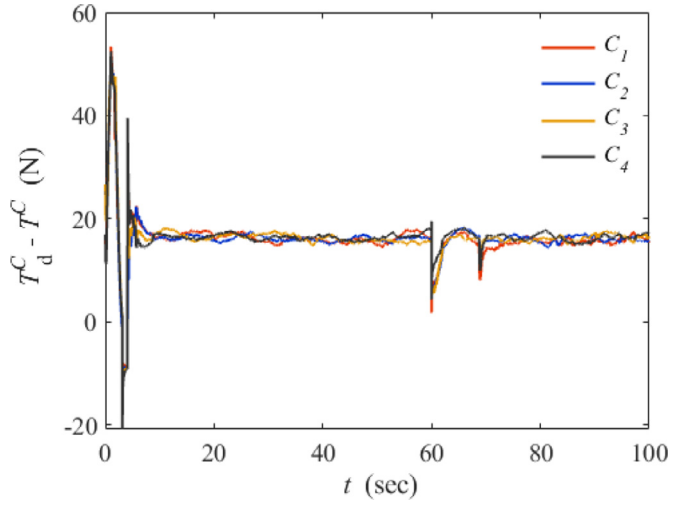

Fig. 8. The deviation of the controller desired tension from the model tension of the cables. (For interpretation of the references to colour in this figure legend, the reader is referred to the web version of this article.)

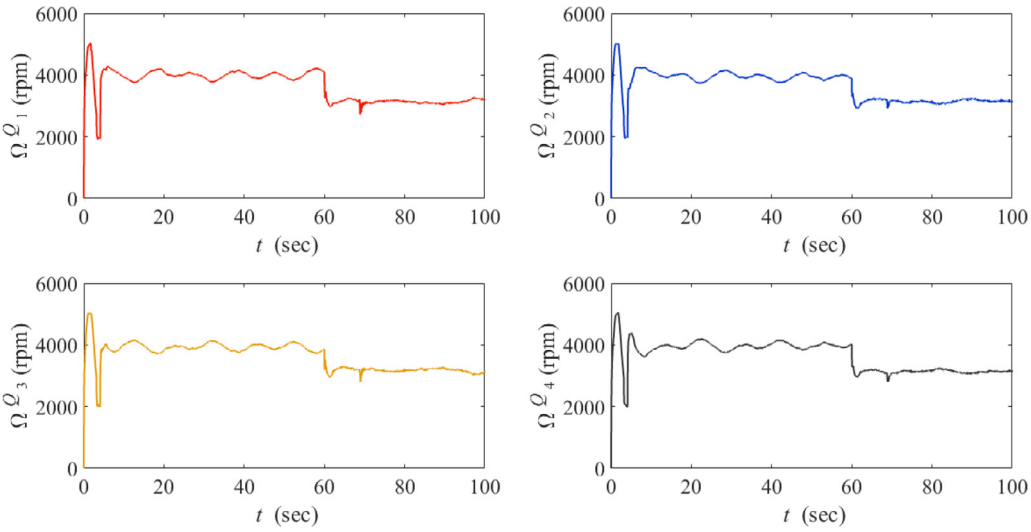

Fig. 9. The average speed of rotors of four quadrotors with the ASM controller.

of the cables in the inertial frame. Thus, the desired angles of each cable are as follows:

$$\phi_{\mathrm{d}}^{\mathcal{C}_1} = -\phi_{\mathrm{d}}^{\mathcal{C}_2} = -\phi_{\mathrm{d}}^{\mathcal{C}_3} = \phi_{\mathrm{d}}^{\mathcal{C}_4} = 25 \text{ deg}$$

These values were chosen to create a fixed square-shaped formation and maintained for the quadrotors during the maneuver. Also, their initial conditions are given by:

$$\theta_{\mathrm{d}}^{\mathcal{C}_1} = \theta_{\mathrm{d}}^{\mathcal{C}_2} = -\theta_{\mathrm{d}}^{\mathcal{C}_3} = -\theta_{\mathrm{d}}^{\mathcal{C}_4} = 25 \text{ deg}$$

These values were chosen to create a fixed square-shaped formation and maintained for the quadrotors during the maneuver. Also, their initial conditions are given by:

$$\phi^{\mathcal{C}_1}(0) = -\phi^{\mathcal{C}_2}(0) = -\phi^{\mathcal{C}_3}(0) = \phi^{\mathcal{C}_4}(0) = 10 \text{ deg}$$

$$\theta^{\mathcal{C}_1}(0) = \theta^{\mathcal{C}_2}(0) = -\theta^{\mathcal{C}_3}(0) = -\theta^{\mathcal{C}_4}(0) = 10 \text{ deg}$$

The controllers' gains of the system are tuned as follows:

$$\boldsymbol{\lambda}_{\mathrm{r}}^{\mathcal{P}} = [1.5,\ 1.5,\ 2.25]^{\mathrm{T}},\ \boldsymbol{\lambda}_{\mathrm{r}}^{\mathcal{Q}_i} = [20,\ 20,\ 20]^{\mathrm{T}},\ \boldsymbol{\lambda}_{\Phi}^{\mathcal{Q}_i} = [60,\ 60,\ 60]^{\mathrm{T}}$$

$$\boldsymbol{\Gamma}_{\mathrm{q_r}}^{\mathcal{P}} = \mathrm{diag}(0.1, 0.1, 0.2),\ \boldsymbol{\Gamma}_{\mathrm{q_r}}^{\mathcal{Q}_i} = 0.1\mathbf{I}_3,\ \boldsymbol{\Gamma}_{\mathrm{q}_\Phi}^{\mathcal{Q}_i} = 0.1\mathbf{I}_3$$

$$\boldsymbol{\Gamma}_{\mathrm{k_r}}^{\mathcal{P}} = 0.002\mathbf{I}_3,\ \boldsymbol{\Gamma}_{\mathrm{k_r}}^{\mathcal{Q}_i} = 0.001\mathbf{I}_3,\ \boldsymbol{\Gamma}_{\mathrm{k}_\Phi}^{\mathcal{Q}_i} = 0.001\mathbf{I}_3$$

$$\boldsymbol{\varepsilon}_{\mathrm{r}}^{\mathcal{P}} = [0.1,\ 0.1,\ 0.2]^{\mathrm{T}},\ \boldsymbol{\varepsilon}_{\mathrm{r}}^{\mathcal{Q}_i} = [1,\ 1,\ 1]^{\mathrm{T}},\ \boldsymbol{\varepsilon}_{\Phi}^{\mathcal{Q}_i} = [0.5,\ 0.5,\ 0.5]^{\mathrm{T}}$$

$$\boldsymbol{\mu}_{\mathrm{r}}^{\mathcal{P}} = [0.5,\ 0.5,\ 0.5]^{\mathrm{T}},\ \boldsymbol{\mu}_{\mathrm{r}}^{\mathcal{Q}_i} = [2,\ 2,\ 2]^{\mathrm{T}},\ \boldsymbol{\mu}_{\Phi}^{\mathcal{Q}_i} = [2,\ 2,\ 2]^{\mathrm{T}}$$

In all subsystems, the initial adaptation gains $\hat{\mathbf{q}}(0)$ and $\hat{\mathbf{k}}(0)$ are equal to $[0.1,\ 0.1,\ 0.1]^{\mathrm{T}}$. The simulation results of Figs. 3-12 show the proper performance of the proposed controller in the payload trajectory tracking and the maintenance of quadrotors formation despite the existence of uncertainties and disturbances mentioned above. Here, an adaptive sliding mode controller is developed to tune the control gains according to an adaptation rule without the upper bound of uncertainties and disturbances information.

Fig. 3 shows the payload trajectory tracking error for the proposed Adaptive Sliding Mode (ASM) controller, which converges to about zero despite the uncertainties and an abrupt change in the payload mass. Although the tracking error of the payload increases at the payload dropping time ($t = 60$ sec), it converges to zero again when the ASM controller gains are tunned by the adaptation law. In general, non-robust controllers such as Feedback Linearization (FL) or PID cannot compensate for excessive uncertainties and disturbances and system parameters changes. Also, if the upper bound of the uncertainties is indeterminate, a robust controller like Sliding Mode (SM) with constant gains cannot wholly compensate for the uncertainties.

The superiority of the proposed method can be better visualized by comparing it with the FL and SM controllers in Table 1. The results of Table 1 are based on the Root-Mean-Squared (RMS) of the payload tracking error, in which the gains of the SM controller are constant and these results. For better analysis, the results of the two cases before and after the payload dropping are presented separately. These results are calculated in 10 to 60 and 70 to 100 s, respectively. Ignoring the first 10 s of each case is because the RMS of the tracking error is independent of the initial conditions.

Since the formation of quadrotors is controlled based on the attitude of the cables relative to the inertial frame, Fig. 4 shows the attitude angles of the cables. Despite the uncertainties and turmoil, the system's performance is proper in making and maintaining quadrotors' formation, and the states $[\phi^{\mathcal{C}_i}, \theta^{\mathcal{C}_i}]^{\mathrm{T}}$ are converged to $[\phi_{\mathrm{d}}^{\mathcal{C}_i}, \theta_{\mathrm{d}}^{\mathcal{C}_i}]^{\mathrm{T}}$. Fig. 5 presents the trajectories of the system (quadrotors and payload), in which making and maintaining the squared-shape formation of the quadrotors is visible in some snapshots.

As mentioned above, the payload attitude is not controlled here, and its values are based on the system's internal dynamic. The payload attitude is bounded during this simulation, as shown in Fig. 6, and oscillates around zero.

The tension force of each cable based on the spring-damper model is illustrated in Fig. 7. Also, the deviation of desired tension from the actual tension of the cables is shown in Fig. 8. This deviation is considered as modeling uncertainty in the system control. The rotors' average speed of each quadrotor, as primarily control input of the system, is shown in Fig. 9. According to the optimization algorithm in the tension distribution, the results indicate the load uniform distribution on all quadrotors after system convergence.

The changes of control gains over time are shown in Figs. 10-12. Since the behavior of the control gains in the quadrotors is similar, only the first quadrotor coefficients are shown for brevity. After the payload dropping time and the increase of the payload position error, the gains will rise again according to the proposed adaptation

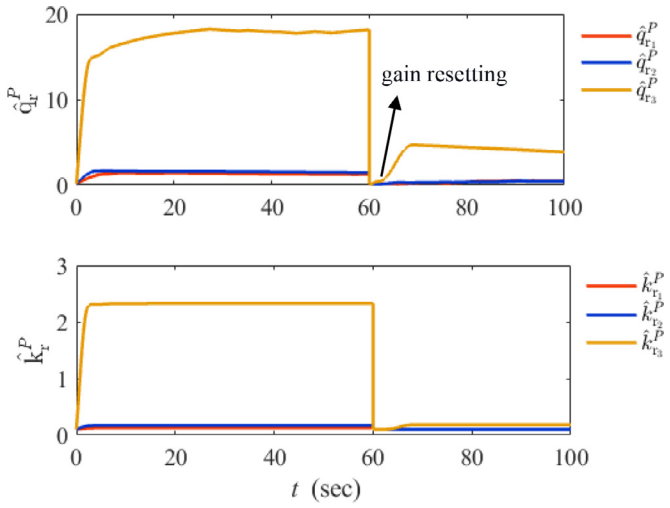

Fig. 10. The adaptation gains in the payload position control.

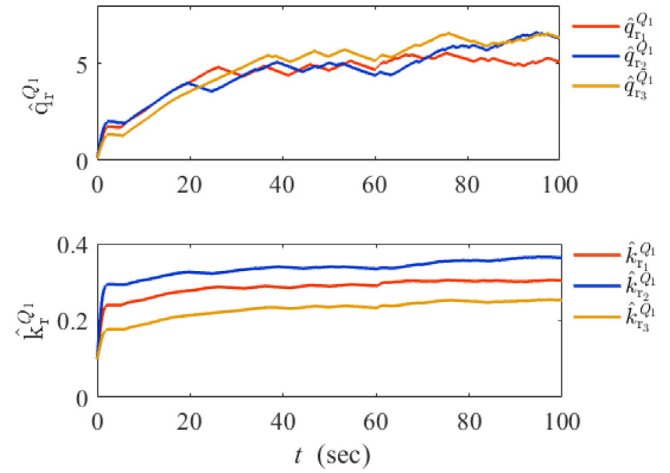

Fig. 11. The adaptation gains in the 1-th quadrotor position control.

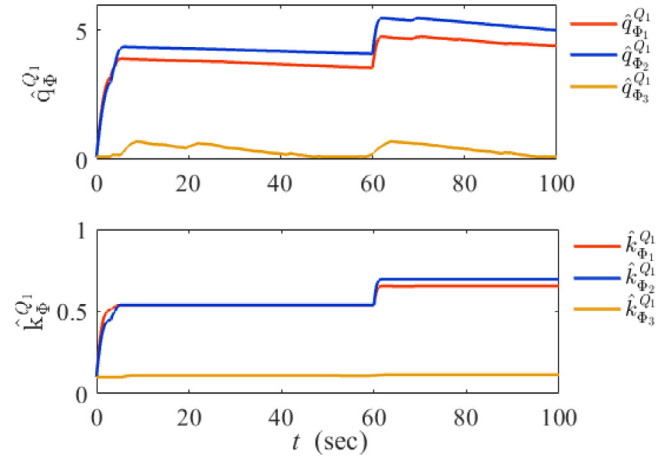

Fig. 12. The adaptation gains in the 1-th quadrotor attitude control.

law. Therefore, this increase can lead to high chatter and saturation of inputs. In order to solve this problem, the gain resetting technique is used here. Thus, after the system parameter changes, the adaptation process is done again by initializing the gains to predetermined small values.

5. Conclusion

This paper presents a three-loop adaptive sliding mode control for trajectory tracking of a cable-suspended rigid body payload carried by multi-quadrotors. A controller has also been proposed to create and maintain the formation of quadrotors during payload transportation so that the load distribution on them is uniform and prevents collisions between them. The proposed controller does not need to know the upper bound of uncertainties and perturbations; the gains of the sliding mode control are estimated according to an adaptation law. The performance of the proposed controller is evaluated in a simulation trial under the simultaneous presence of high uncertainty in the mass properties of the system, the presence of external disturbances, and abrupt change in the mass of the payload, which results in a proper outcome. The system's overall stability has been theoretically proven by Lyapunov theory and the multiple time scale principle.

Declaration of Competing Interest

The authors declare that they have no known competing financial interests or personal relationships that could have appeared to influence the work reported in this paper.

References

[1] Y. Alothman, M. Guo, D. Gu, Using iterative LQR to control two quadrotors transporting a cable-suspended load, IFAC-PapersOnLine 50 (2017), doi:10.1016/j.ifacol.2017.08.861.
[2] S.O. Ariyibi, O. Tekinalp, Quaternion-based nonlinear attitude control of quadrotor formations carrying a slung load, Aerosp. Sci. Technol. 105 (2020), doi:10.1016/j.ast.2020.105995.
[3] J. Arora, Introduction to optimum design. 2012. doi:10.1016/C2009-0-61700-1.
[4] S.P. Bhat, D.S. Bernstein, Finite-time stability of continuous autonomous systems, SIAM J. Control. Optim. 38 (2000), doi:10.1137/S0363012997321358.
[5] G.A. Cardona, D. Tellez-Castro, E. Mojica-Nava, Cooperative transportation of a cable-suspended load by multiple quadrotors, IFAC-PapersOnLine 52 (2019), doi:10.1016/j.ifacol.2019.12.149.
[6] T. Chen, J. Shan, A novel cable-suspended quadrotor transportation system: from theory to experiment, Aerosp. Sci. Technol. 104 (2020), doi:10.1016/j.ast.2020.105974.
[7] S. Dai, T. Lee, D.S. Bernstein, Adaptive control of a quadrotor UAV transporting a cable-suspended load with unknown mass, in: Proc. IEEE Conf. Decis. Control, vol. 2015- February, 2014, doi:10.1109/CDC.2014.7040352.
[8] K.K. Dhiman, M. Kothari, A. Abhishek, Autonomous load control and transportation using multiple quadrotors, J. Aerosp. Inf. Syst. 17 (2020), doi:10.2514/1.I010787.
[9] Q. Dong, Q. Zong, B. Tian, F. Wang, Adaptive-gain multivariable super-twisting sliding mode control for reentry RLV with torque perturbation, Int. J. Robust. Nonlin. Control. 27 (2017), doi:10.1002/rnc.3589.
[10] J. Geng, J.W. Langelaan, Implementation and demonstration of coordinated transport of a slung load by a team of rotorcraft, in: AIAA Scitech 2019 Forum, 2019, doi:10.2514/6.2019-0913.
[11] J. Geng, J.W. Langelaan, Cooperative transport of a slung load using load-leading control, J. Guid. Control. Dyn. 43 (2020), doi:10.2514/1.G004680.
[12] J. Gimenez, D.C. Gandolfo, L.R. Salinas, C. Rosales, R. Carelli, Multi-objective control for cooperative payload transport with rotorcraft UAVs, ISA Trans. 80 (2018), doi:10.1016/j.isatra.2018.05.022.
[13] F.A. Goodarzi, T. Lee, Stabilization of a rigid body payload with multiple cooperative quadrotors, J. Dyn. Syst. Meas. Control. Trans. ASME 138 (2016), doi:10.1115/1.4033945.
[14] Q. Jiang, V. Kumar, The inverse kinematics of cooperative transport with multiple aerial robots, IEEE Trans. Robot. 29 (2013), doi:10.1109/TRO.2012.2218991.
[15] K. Klausen, C. Meissen, T.I. Fossen, M. Arcak, T.A. Johansen, Cooperative control for multirotors transporting an unknown suspended load under environmental disturbances, IEEE Trans. Control. Syst. Technol. 28 (2020), doi:10.1109/TCST.2018.2876518.
[16] K. Kotani, Z. Guo, T. Namerikawa, Z. Qu, Cooperative transport control by a multicopter system, IET Control. Theory Appl. 15 (2021), doi:10.1049/cth2.12089.
[17] J.S Kowalik, Practical optimization (Philip E. Gill, Walter Murray and Margaret H. Wright), SIAM Rev. 25 (1983), doi:10.1137/1025065.
[18] T. Lee, Geometric Control of Quadrotor UAVs Transporting a Cable-Suspended Rigid Body, IEEE Trans. Control. Syst. Technol. 26 (2018), doi:10.1109/TCST.2017.2656060.
[19] H. Lee, H.J. Kim, Constraint-based cooperative control of multiple aerial manipulators for handling an unknown payload, IEEE Trans. Ind. Inform. 13 (2017), doi:10.1109/TII.2017.2692270.

[20] Z. Li, J. Erskine, S. Caro, A. Chriette, Design and control of a variable aerial cable towed system, IEEE Robot. Autom. Lett. 5 (2020), doi:10.1109/LRA.2020.2964165.
[21] G. Li, R. Ge, G. Loianno, Cooperative transportation of cable suspended payloads with MAVs using monocular vision and inertial sensing, IEEE Robot. Autom. Lett. 6 (2021), doi:10.1109/LRA.2021.3065286.
[22] X. Liang, Y. Fang, N. Sun, H. Lin, X. Zhao, Adaptive nonlinear hierarchical control for a rotorcraft transporting a cable-suspended payload, IEEE Trans. Syst. Man Cybern. Syst. (2019), doi:10.1109/tsmc.2019.2931812.
[23] C. Masone, H.H. Bülthoff, P. Stegagno, Cooperative transportation of a payload using quadrotors: a reconfigurable cable-driven parallel robot, in: IEEE Int. Conf. Intell. Robot. Syst., vol. 2016- November, 2016, doi:10.1109/IROS.2016.7759262.
[24] D. Mellinger, M. Shomin, N. Michael, V. Kumar, Cooperative grasping and transport using multiple quadrotors, Springer Tracts Adv. Robot. 83 STAR (2012), doi:10.1007/978-3-642-32723-0_39.
[25] Y. Naidoo, R. Stopforth, G. Bright, Quad-rotor unmanned aerial vehicle helicopter modelling & control, Int. J. Adv. Robot. Syst. 8 (2011), doi:10.5772/45710.
[26] I.H.B. Pizetta, A.S. Brandão, M. Sarcinelli-Filho, Avoiding obstacles in cooperative load transportation, ISA Trans. 91 (2019), doi:10.1016/j.isatra.2019.01.019.
[27] F. Plestan, Y. Shtessel, V. Bregeault, A. Poznyak, New methodologies for adaptive sliding mode control, Int. J. Control. 83 (2010), doi:10.1080/00207179.2010.501385.
[28] J.G. Romero, H. Rodríguez-Cortés, Asymptotic stability for a transformed nonlinear UAV model with a suspended load via energy shaping, Eur. J. Control. 52 (2020), doi:10.1016/j.ejcon.2019.09.002.
[29] V.N. Sankaranarayanan, S. Roy, S. Baldi, Aerial transportation of unknown payloads: adaptive path tracking for quadrotors, in: IEEE Int. Conf. Intell. Robot. Syst., 2020, doi:10.1109/IROS45743.2020.9341402.
[30] B. Shirani, M. Najafi, I. Izadi, Cooperative load transportation using multiple UAVs, Aerosp. Sci. Technol. 84 (2019), doi:10.1016/j.ast.2018.10.027.
[31] I.A. Shkolnikov, Y.B. Shtessel, A multiple-loop sliding mode control system with second-order boundary layer dynamics, IFAC Proc. Vol. 35 (2002), doi:10.3182/20020721-6-es-1901.01097.
[32] B. Sumantri, N. Uchiyama, S. Sano, Least square based sliding mode control for a quad-rotor helicopter and energy saving by chattering reduction, Mech. Syst. Signal. Process. (2016) 66–67, doi:10.1016/j.ymssp.2015.05.013.
[33] Y.H. Tan, S. Lai, K. Wang, B.M. Chen, Cooperative control of multiple unmanned aerial systems for heavy duty carrying, Annu. Rev. Control. 46 (2018), doi:10.1016/j.arcontrol.2018.07.001.
[34] S. Thapa, H. Bai, J. Acosta, Cooperative aerial manipulation with decentralized adaptive force-consensus control, J. Intell. Robot. Syst. Theory Appl. 97 (2020), doi:10.1007/s10846-019-01048-4.
[35] D.K.D. Villa, A.S. Brandao, R. Carelli, M. Sarcinelli-Filho, Cooperative load transportation with two quadrotors using adaptive control, IEEE Access 9 (2021), doi:10.1109/ACCESS.2021.3113466.
[36] H. Yang, D. Lee, Hierarchical cooperative control framework of multiple quadrotor-manipulator systems, Proc. - IEEE Int. Conf. Robot. Autom. 2015-June (2015), doi:10.1109/ICRA.2015.7139844.
[37] S. Yang, B. Xian, Energy-based nonlinear adaptive control design for the quadrotor UAV system with a suspended payload, IEEE Trans. Ind. Electron. 67 (2020), doi:10.1109/TIE.2019.2902834.